Eur Biophys J (2012) 41:27–39
DOI 10.1007/s00249-011-0755-7

ORIGINAL PAPER

EBSA
Biophysics in Europe

How does the ryanodine receptor in the ventricular myocyte wake up: by a single or by multiple open L-type Ca^{2+} channels?

Thomas Schendel · Rüdiger Thul · James Sneyd · Martin Falcke

Received: 2 February 2011 / Revised: 23 August 2011 / Accepted: 14 September 2011 / Published online: 1 October 2011

Abstract We study here the early stage of Ca^{2+}-induced Ca^{2+} release (CICR) in the diadic cleft of cardiac ventricular myocytes. A crucial question for this mechanism is whether the activation of the ryanodine receptors (RyRs) is triggered by one or by multiple open L-type Ca^{2+} channels (LCCs). We address the problem through a modelling approach that allows us to investigate both possibilities. The model is based on a spatially resolved description of a Ca^{2+} release unit (CaRU), consisting of the junctional sarcoplasmic reticulum and the diadic cleft, with well-defined channel placement. By taking advantage of largely varying time scales of the Ca^{2+} dynamics in the diadic cleft, the governing equations can be reduced to one ordinary differential equation that describes the Ca^{2+} fluxes, the electric field due to surface charges and diffusion. Our study shows that the mechanisms of the early stage of CICR shape measurable properties of CICR in a characteristic way. From here we conclude that the activation of RyRs requires multiple open LCCs.

Keywords Calcium-induced calcium release · Signalling micro-domain · Calcium dynamics · Mathematical modelling

Introduction

Ca^{2+}-induced Ca^{2+} release (CICR) is the central step of excitation–contraction coupling (ECC) in cardiac myocytes (Bers et al. 2002). In ventricular myocytes, CICR is controlled locally by the co-localization of L-type Ca^{2+}-channels (LCCs) in the T-tubule membrane on the one side of a diadic cleft and ryanodine receptor channels (RyRs) in the sarcoplasmic reticulum (SR) membrane on the other side. Depolarisation of the plasma membrane leads to activation of L-type Ca^{2+}-channels, which in turn causes Ca^{2+} entry from the extracellular space into the diadic cleft. The influx of Ca^{2+} activates RyRs at the junctional sarcoplasmic reticulum (JSR), which release Ca^{2+} from the SR. Subsequently, the Ca^{2+} concentration in the diadic cleft increases substantially, while the JSR partially depletes. The small distances within the diadic cleft of $\sim$15 nm (Franzini-Armstrong et al. 1999) provide a strong coupling between membrane depolarisation and Ca^{2+} release (the volume of a cleft is in the range of 10^{-18} l).

To date, many details of CICR remain still unclear. For example, how does luminal Ca^{2+} in the JSR affect the gating of RyRs (Györke et al. 2002)? How does the huge variation in cleft sizes [resulting in a high variability of the number of RyRs per RyR cluster as reported by Baddeley et al. (2009)] affect CICR? What role do electrostatic effects due to surface charges play in this process? Even the LCC–RyR coupling details are controversially discussed. Can the opening of one LCC trigger the opening of RyRs in a reliable manner? Former studies, e.g. by Adachi-Akahane et al. (1999), Song et al. (2001) and Altamirano

Electronic supplementary material The online version of this article (doi:10.1007/s00249-011-0755-7) contains supplementary material, which is available to authorized users.

T. Schendel (✉) · M. Falcke
Max Delbrück Center of Moleculare Medicine,
Robert-Rössle-Str. 10, 13092 Berlin, Germany
e-mail: thomas.schendel@mdc-berlin.de

R. Thul
School of Mathematical Sciences,
University of Nottingham, Nottingham, UK

J. Sneyd
Department of Mathematics, University of Auckland,
Auckland, New Zealand

and Bers (2007), suggest that the coupling fidelity (the probability that one open LCC triggers the opening of a RyR) appears to be high, while other investigations (Polakova et al. 2008) claim that the coupling fidelity is low and that consequently the simultaneous opening of several LCCs is required to activate the RyRs.

In this study we identify qualitative differences between experimental features of CICR as observed in two scenarios: firstly that the opening of a RyR is triggered by just one open LCC, and secondly that multiple LCCs have to open simultaneously in order to induce Ca^{2+} liberation from the SR. Both cleft models reproduce approximately measured gain and gradedness, have the same gain at membrane potential of 0 mV, show similar distributions of the maximal number of open RyR during a spark and exhibit very similar influx through LCCs (Figs. 6–11, and Supplementary Material Fig. 1). We rendered models comparable in these properties since no obvious difference between cleft behaviour with high and low coupling fidelity with respect to them has been observed experimentally. These criteria entail changes in several parameter when going from one model to the other. We take into account varying size of the diadic cleft and number of RyRs inside it and the electric field in the cleft due to surface charges. Our analysis is based on the extension of a previously developed model (Schendel and Falcke 2009), which now describes the cleft three-dimensionally with a defined channel placement. The channel gating is modelled in a stochastic manner. We also take into account the Ca^{2+} dynamics in the JSR and its influence on the gating of the RyR.

Methods

The model of the local calcium release unit (CaRU) consists of three compartments: the diadic cleft, the JSR and the cytosolic bulk (Fig. 1). The RyRs at the JSR are co-localized to the LCC in the membrane of the T-tubules. We assume the diadic cleft to be a cylinder with height of 15 nm (Soeller and Cannel 1997). The dynamics of the CaRU results from three different contributions: the gating of the channel states (of the LCCs and RyRs), the Ca^{2+} distribution in the diadic cleft and the Ca^{2+} dynamics in the JSR.

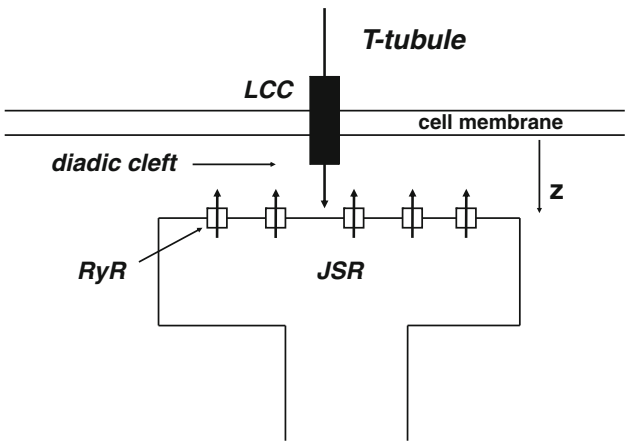

Fig. 1 Scheme of the local CaRU, consisting of the diadic cleft and the JSR. RyRs and LCCs are co-localized

Channel placement and gating

For studying the case that one conducting LCC triggers the opening of RyRs—which we will refer to as the MIN model—we choose a ratio of LCCs to RyRs of approximately 1:4 (Wang et al. 2001). When we investigate the case that several open LCCs are required to activate the RyRs, we increase the LCC-to-RyR ratio to 1:1 (MAX model). More precisely, 82% of initial RyR activation was triggered while a single LCC was open in the MIN model, while in the MAX model 78% of RyR activation occurred with more than one LCC open. Although there is no direct experimental evidence for the LCC-to-RyR ratio of 1:1 in the MAX model, detailed measurements have shown that (a) the LCC-to-RyR ratio is 1:4–7 (Wang et al. 2001; Bers and Stiffel 1993); (b) the average number of RyRs in a RyR cluster is 13.6 (Baddeley et al. 2009); and (c) multiple simultaneously open LCCs are necessary to trigger the opening of RyRs (Polakova et al. 2008). Clearly, these experimental results contradict each other, indicating at the same time that one or more LCCs could be involved in activating RyRs. We will investigate here whether characteristic properties that can be measured at the cell level favour either the case that one single LCC triggers the opening of RyRs or the case that multiple open LCCs are required to activate Ca^{2+} release from the JSR (Tables 1, 2).

Table 1 RyR and LCC parameters

RyR parameter	Value	LCC parameter	Value
g	4 $\mu m^3\ s^{-1}$	V_L	−2 mV
k_{om}	60 s^{-1}	ΔV_L	7 mV
k_{im}	5 s^{-1}	ϕ_L	6.667
k_{ac}^{max}	928.8 s^{-1}	t_L	0.0033 s
k_{ac}^{max}	7.9 s^{-1}	τ_L	0.65 s
K_{JSR}	550 μM	K_L	0.22 μM
λ	27.5	a	0.0625
		b	14

Table 2 Remaining channel parameters

Parameter	Value (MIN model)	Value (MAX model)
J_L	0.23 $\mu m^3\ s^{-1}$	0.05 $\mu m^3\ s^{-1}$
K_{ac}	8.5 μM	3 μM
K_{in}	8.5 μM	3 μM

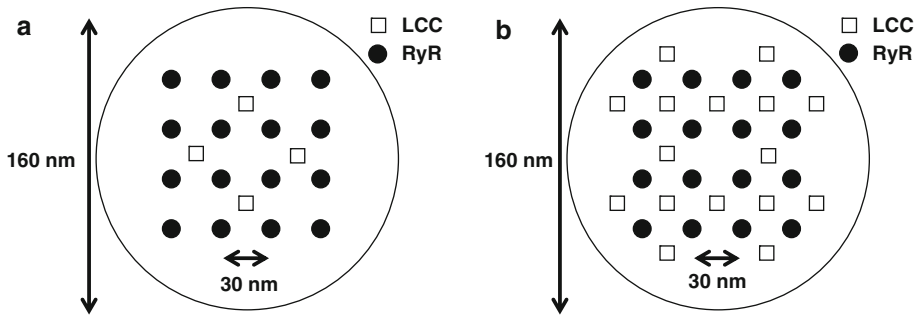

Fig. 2 Channel placement of 16 RyRs and **a** 4 LCCs in the MIN model and **b** 16 LCCs in the MAX model

RyRs are known to form regular arrays, with centre-to-centre spacing of approximately 30 nm (Franzini-Armstrong and Protasi 1997; Baddeley et al. 2009). For computational convenience, we place the LCCs such that they have the same distance to the four nearest RyRs (Fig. 2). When the membrane is depolarised to 0mV, a single LCC suffices to activate the RyRs in the MIN model, while two open LCCs are required to trigger Ca^{2+} liberation from the SR in the MAX model. We also vary the number of RyRs to account for the high variability of RyR expression in the diadic cleft.

Baddeley et al. (2009) report that the number of RyRs per RyR cluster is exponentially distributed, with an average of 13.6 RyRs per cluster. However, it is not clear if one diadic cleft contains only one or several RyR clusters. Since we are mainly interested in the direct coupling between RyRs and the co-localized LCCs, we assume that each diadic cleft contains one RyR cluster. We use diadic clefts with quadratic numbers of RyRs 1, 4, 9, 16,…,100 that implement the findings of Baddeley et al. (2009). Note that for the MIN model we do not consider diadic clefts with only one RyR, since the LCC-to-RyR ratio of 1:4 cannot be achieved for integer channel numbers in this case. The radii and the probability distribution of the cleft sizes are listed in Tables 3 and 4.

For the LCC state dynamics we employ the kinetic scheme from Hinch et al. (2004), which is a lumped state model. It consists of three states: open, closed and inactivated (Fig. 3). Inactivation is Ca^{2+} dependent in this scheme, and the rates have the following form (Hinch et al. 2004):

$$k_{\mathrm{CO}} = \frac{e^{\frac{V-V_L}{dV_L}}}{t_L\left(e^{\frac{V-V_L}{dV_L}}+1\right)},$$

$$k_{\mathrm{OC}} = \frac{\phi_L}{t_L},$$

$$k_{\mathrm{CI}} = c_{\mathrm{di}}\frac{e^{\frac{V-V_L}{dV_L}}+a}{K_L\tau_L\left(e^{\frac{V-V_L}{dV_L}}+1\right)},$$

$$k_{\mathrm{IC}} = b\frac{e^{\frac{V-V_L}{dV_L}}+a}{\tau_L\left(e^{\frac{V-V_L}{dV_L}}+1\right)},$$

where V and c_{di} denote the membrane potential and the Ca^{2+} concentration in the diadic cleft, respectively. For all other parameters, see Hinch et al. (2004).

For the RyRs we adapt a scheme originally developed in Tang and Othmer (1994) (Fig. 4). It consists of a rest state, an open state and two inactivated states. The rate to inactivation depends on the Ca^{2+} concentration in the diadic cleft, and the opening rate of the channel is a nonlinear function of the subsarcolemmal Ca^{2+} concentration. We change this description to account for four findings: Firstly, the activation of the RyR is a fourth-order process (Polakova et al. 2008). Secondly, the Ca^{2+}-dependent rates should saturate at a finite value for high Ca^{2+} concentrations in the cleft. That is why we use Hill functions for the

Table 3 Radii of diadic clefts

Number of RyRs	Radii (nm)
1	35
4	45
9	70
16	80
25	100
36	120
49	140
64	165
81	190
100	210

Table 4 Distribution of cleft sizes for the MIN and MAX model

Number of RyRs	Probability (MIN) (%)	Probability (MAX) (%)
1	0	13.68
4	35.67	22.00
9	25.88	22.95
16	18.61	20.03
25	10.33	11.12
36	5.27	6.00
49	2.83	2.72
64	1.00	1.05
81	0.30	0.34
100	0.11	0.12

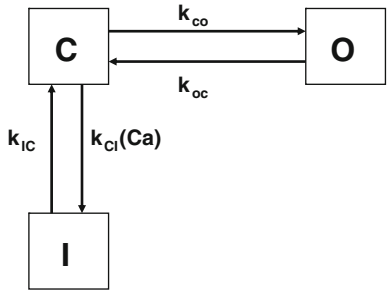

Fig. 3 Kinetic scheme for the LCC from Hinch et al. (2004). This scheme is a simplification of a more complex model. *O* open, *C* closed, *I* inactivated state

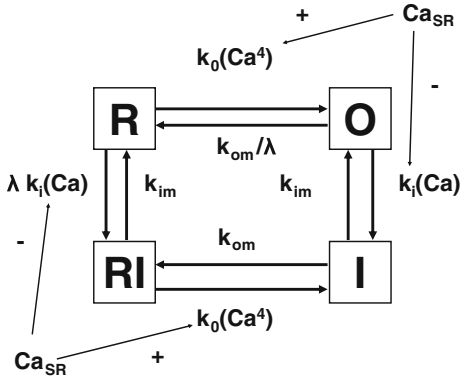

Fig. 4 Kinetic scheme for the RyR from Tang and Othmer (1994). *O* open, *C* closed, *I* inactivated, *R* resting state. Activation is a nonlinear function of Ca^{2+}; inactivation is Ca^{2+} dependent. The Ca^{2+}-dependent rates are influenced by the Ca^{2+} concentration in the JSR

Ca^{2+}-dependent rates. For the activation process, it was shown that this fits the experimental data (Sobie et al. 2002). Thirdly, we implement an asymmetry in the inactivation process, making the inactivation rate higher in case the RyR is closed. To obey microreversibility, we also introduce this term in the rate from the open to the rest state. Such an asymmetric inactivation is also used in Wang et al. (2004). Fourthly, since the Ca^{2+} concentration in the JSR also influences RyR gating (Györke et al. 2002), the original scheme (Tang and Othmer 1994) is modified according to the study of Shannon et al. (2004). The rates that depend on Ca^{2+} in the diadic cleft are modulated by the luminal concentration as follows:

$$\begin{aligned} k_{\mathrm{JSR}} &= \left(15 - \frac{14}{1 + \left(\frac{K_{\mathrm{JSR}}}{c_{\mathrm{JSR}}}\right)^3}\right), \\ k_0 &= \frac{k_{\mathrm{ac}}^{\max} \frac{c_{\mathrm{di}}^4}{c_{\mathrm{di}}^4 + K_{\mathrm{ac}}^4}}{k_{\mathrm{JSR}}}, \\ k_i &= k_{\mathrm{in}}^{\max} \frac{c_{\mathrm{di}}}{c_{\mathrm{di}} + K_{\mathrm{in}}} k_{\mathrm{JSR}}. \end{aligned} \tag{1}$$

In case of a depleted JSR, the probability of opening the RyRs decreases, while the rate of Ca^{2+}-dependent inactivation increases. We refer the reader to the Supplementary Material for details on how we fit the RyR parameter values.

We model the channel gating in a stochastic manner due to the experimental fact that a Ca^{2+} release event (Ca^{2+} spark) involves only 1–7 open RyRs (Wang et al. 2004). More details about the specific numerical scheme are provided in section "Matching the dynamics together".

Concentration profile in the diadic cleft

We take into account the Ca^{2+} fluxes from LCCs and RyRs, Ca^{2+} diffusion and the effect of the membrane surface charges. We describe the Ca^{2+} channels as point sources $\mathbf{r}_i = (z_i, r_i, \varphi_i)$ located at positions with either a flux J_{LCC}^i or a flux J_{RyR}^i in the diadic cleft. The dynamics of the Ca^{2+} concentration in the diadic cleft c_{di} is then given by

$$\frac{\partial c_{\mathrm{di}}}{\partial t} = \sum_i J_{\mathrm{LCC}}^i + \sum_j J_{\mathrm{RyR}}^j + D_c \Delta_{r,\varphi} c_{\mathrm{di}}(\mathbf{r}) - \frac{\partial}{\partial z} J_z. \tag{2}$$

Here, D and $\Delta_{r,\phi}$ denote the diffusion coefficient of Ca^{2+} in the cytosol and the r and ϕ dependence of the Laplace operator in cylindrical coordinates, respectively. Following Langer and Peskoff (1996) we use a reduced value for the diffusion coefficient of $D = 100\ \mu\mathrm{m}^2\ \mathrm{s}^{-1}$ to account for the effect of the spatial dimension of the RyRs. The flux density

$$J_z = -D\left(\frac{\partial c_{\mathrm{di}}}{\partial z} + 2c_{\mathrm{di}} \frac{\mathrm{d}\phi}{\mathrm{d}z}\right) \tag{3}$$

models the effect of the Nernst–Planck electro-diffusion in the z-direction. The dimensionless electrical potential $\phi = \psi e/(k_{\mathrm{B}}T)$ is derived from the membrane potential ψ, the unit electrical charge e, Boltzmann's constant k_{B} and the absolute temperature T. Note that z is the direction from the T-tubule membrane to the JSR (Fig. 1, Table 5).

We assume quasi-stationarity of the Ca^{2+} concentration profile in the diadic cleft, since the time to reach the steady state is much smaller than the typical time scale for channel gating (Hake and Lines 2008; Soeller and Cannel 1997).

Table 5 Other parameters

Parameter	Value	Parameter	Value
c_{ext}	1,000 μM	k_{M}^+	100 μ M^{-1} s^{-1}
c_{NSR}	700 μM	k_{M}^-	38 s^{-1}
D_c	100 $\mu\mathrm{m}^2$ s^{-1}	k_{T}^+	40 $\mu\mathrm{M}^{-1}\mathrm{s}^{-1}$
B_{CSQN}	400 μM	k_{T}^-	40 s^{-1}
K_c	600 μM	B_M	24 μM
n	15	B_T	70 μM
τ_{refill}	7.5 ms	ρ_{SERCA}	390 s^{-1}

In order to solve the time-independent version of Eq. 2, we make the ansatz

$$c_{\mathrm{di}}(r,\varphi,z) = f(r,\varphi)Z(z). \tag{4}$$

Note that Eq. 2 is not separable and that this ansatz will not solve it exactly. An estimation of the error generated by this ansatz is presented in the Supplementary Material. We identify $Z(z)$ with the z-dependence of the Ca^{2+} concentration arising from the electric field. We here make the assumption that the Ca^{2+} concentration in the diadic cleft is independent of the z-coordinate in the absence of an electric field due to the large diffusion coefficient of free Ca^{2+} ($D = 100\ \mu m^2\ s^{-1}$) and the small height of the cleft ($h = 15$ nm). This is very well justified by a comparison between the approximate and the exact stationary solution with a single open channel provided in the Supplementary Material.

Inserting Eq. 4 into Eq. 2, we find in the case when all channels are closed that

$$-\frac{\Delta_{r,\varphi} f}{f} = \frac{1}{Z}\frac{\mathrm{d}}{\mathrm{d}z}\left(\frac{\mathrm{d}Z}{\mathrm{d}z} + 2Z\frac{\mathrm{d}\phi}{\mathrm{d}z}\right) = \rho, \tag{5}$$

where ρ presents the separation constant. In order to determine $Z(z)$, we can rewrite Eq. 5 by using Eq. 3 as

$$-\frac{1}{D}\frac{\mathrm{d}}{\mathrm{d}z}J_z = \frac{\mathrm{d}}{\mathrm{d}z}\left(\frac{\mathrm{d}Z}{\mathrm{d}z} + 2Z\frac{\mathrm{d}\phi}{\mathrm{d}z}\right) = \rho Z, \tag{6}$$

subject to the boundary conditions (Jayasinghe et al. 2009; Scriven et al. 2000)

$$J_z(z=0) = J_z(z=h) = 0. \tag{7}$$

Since $Z(z) > 0$ for all z, J_z is a strictly monotonically decreasing function of z for $\rho > 0$ and a strictly monotonically increasing function of z for $\rho < 0$. In both cases, J_z does not satisfy the boundary conditions in Eq. (7), because a strictly monotone function cannot have two roots. Therefore, ρ needs to vanish and we are left with

$$\frac{\mathrm{d}}{\mathrm{d}z}\left(\frac{\mathrm{d}Z}{\mathrm{d}z} + 2Z\frac{\mathrm{d}\phi}{\mathrm{d}z}\right) = 0. \tag{8}$$

Following the work by Soeller and Cannel (1997), we assume for the electric field ϕ the z-dependence

$$\phi(z) = \phi_0 \mathrm{e}^{-\kappa z}, \tag{9}$$

where $1/\kappa$ corresponds to the Debye length and ϕ_0 denotes the electric potential at the sarcolemmal membrane ($z = 0$). From Soeller and Cannel (1997), we have $\phi_0 = -2.2$ and $\kappa = 1\ \mathrm{nm}^{-1}$. Inserting Eq. 9 into Eq. 8 leads to the solution

$$Z(z) = C_0 \mathrm{e}^{-2\phi_0 \mathrm{e}^{-\kappa z}}. \tag{10}$$

Since $Z(z) = 1$ for all z in the absence of an electric field, we find $C_0 = 1$. The Ca^{2+} concentration profile in the z-direction computed from Eq. 10 is shown in Fig. 5.

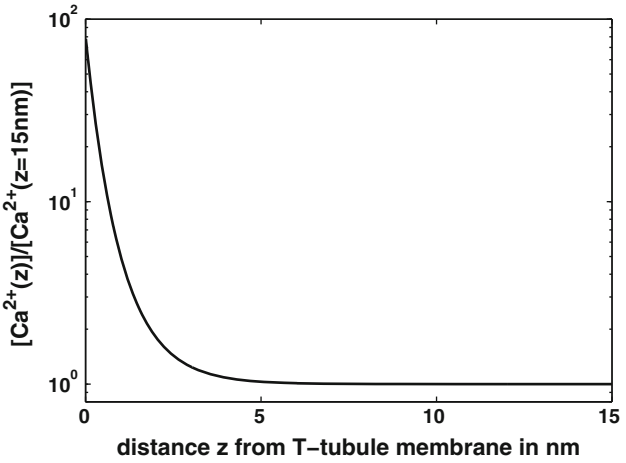

Fig. 5 z-Dependence of the Ca^{2+} concentration profile. The maximum is located close to the sarcolemma membrane

In the next step, we determine $f(r, \varphi)$. The Ca^{2+} fluxes through the LCCs (which we model by the Goldman–Hodgkin–Katz equation) and RyRs are given by

$$J^i_{\mathrm{LCC}} = J_L \delta V \frac{c_{\mathrm{ext}}\mathrm{e}^{-\delta \mathrm{V}} - \mathrm{c}^{\mathrm{i}}_{\mathrm{di}}}{1 - \mathrm{e}^{-\delta V}}, \tag{11a}$$

$$J^i_{\mathrm{RyR}} = g(c_{\mathrm{JSR}} - c^i_{\mathrm{di}}), \tag{11b}$$

where $\delta = \frac{2F}{RT}$, $c^i_{\mathrm{di}} = c_{\mathrm{di}}(\mathbf{r}_i)$ and $c^{\max}_{\mathrm{ac}} = c_{\mathrm{JSR}}(\mathbf{r}_i)$. c_{JSR} and c_{ext} denote the Ca^{2+} concentration in the JSR and the external Ca^{2+} concentration, respectively. For the time being, we assume that the Ca^{2+} concentration at the border of the diadic cleft, c_{bulk}, is constant, i.e.

$$f(r = R, \varphi) = c_{\mathrm{bulk}}, \qquad 0 \le \varphi \le 2\pi, \tag{12}$$

and we will discuss this assumption at the end of this section. To determine $f(r, \varphi)$, we insert Eq. 4 into Eq. 2, integrate over z and divide by $\int_0^h Z(z)\mathrm{d}z$:

$$0 = \frac{1}{h^*}\sum_i J^i_{\mathrm{LCC}}(r_i, \varphi_i, z_{\mathrm{L}}) + \frac{1}{h^*}\sum_j J^j_{\mathrm{RyR}}(r_j, \varphi_j, z_{\mathrm{R}}) + D\Delta_{r,\varphi} f(r, \varphi). \tag{13}$$

Here, we introduce an effective height

$$h^* = \int_0^h Z(z)\mathrm{d}z, \tag{14}$$

which is equal to h in the absence of an electric field. For $h > 5$ nm, we obtain approximately the following relation:

$$h^* = h + 24\,\mathrm{nm}. \tag{15}$$

Note that the LCCs and RyRs are positioned at distances z_{L} and z_{R} from the sarcolemmal membrane, respectively. We set $z_{\mathrm{L}} = 1.5$ nm, and choose a value for $z_{\mathrm{R}} > z_{\mathrm{L}}$ such that $Z(z_{\mathrm{R}}) \approx 1$.

To solve Eq. 13, we make use of the fact that the fluxes $J_{\mathrm{ac}}^{\max}$ and J_{RyR}^{i} in Eq. 11a, b are constant for a fixed number of conducting channels due to the stationarity of the Ca^{2+} concentration profile. Therefore, we can determine the Ca^{2+} concentration in the diadic cleft and hence the currents self-consistently by starting from some initial values for $J_{\mathrm{ac}}^{\max}$ and J_{RyR}^{i} and then compute the resulting Ca^{2+} concentration, which in turn gives rise to an updated value of the Ca^{2+} fluxes. For constant fluxes $J_{\mathrm{ac}}^{\max}$ and J_{RyR}^{i}, the Ca^{2+} concentration in the diadic cleft is given by

$$c_{\mathrm{di}}(\mathbf{r}) - \Omega(z) = \sum_{i=1}^{N_{\mathrm{RyR}}} \gamma_i J_{\mathrm{RyR}}^{i} \eta(\mathbf{r_i}, \mathbf{r}) + \sum_{j=1}^{N_{\mathrm{LCC}}} \gamma_j J_{\mathrm{LCC}}^{j} \eta(\mathbf{r_j}, \mathbf{r}), \tag{16}$$

with

$$\eta(\mathbf{r}_i, \mathbf{r}) = \frac{Z(z)}{h^* \pi D} \left\{ \sum_{k=0}^{\infty} \frac{B_0\left(x_{0,k}\frac{r_i}{R}\right) B_0\left(x_{0,k}\frac{r}{R}\right)}{x_{0,k}^2 B_1^2\left(x_{0,k}\right)} + 2\sum_{n=1}^{\infty}\sum_{k=0}^{\infty} \frac{B_n\left(x_{n,k}\frac{r_i}{R}\right) B_n\left(x_{n,k}\frac{r}{R}\right)\cos(n\varphi)}{x_{n,k}^2 B_{n+1}^2\left(x_{n,k}\right)} \right\}, \tag{17}$$

and

$$\Omega(z) = (c_{\mathrm{bulk}} - c_{\mathrm{rest}}) Z(z) + c_{\mathrm{rest}}. \tag{18}$$

B_n denotes the Bessel function of order n, and $x_{n,k}$ corresponds to the kth root of B_n. The indicator function $\gamma_i = 1$ if the ith channel is open and 0 otherwise.

The solution for c_{di} diverges at $r = r_i$ and $\varphi = \varphi_i$ due to the δ-function approximation for the channels. This prevents us from calculating the Ca^{2+} concentrations at the channels, which is necessary for determining the currents in Eq. 11a, b. To circumvent these divergences, we firstly compute the average Ca^{2+} concentration $\overline{c}$ from the concentration profile $c(r)$ over the Donnan potential range of the channel [see Mejia-Alvarez et al. (1999) for the definition of the Donnan potential range of a RyR]. The reason for choosing the Donnan potential range lies in the fact that we are only guaranteed the validity of cytosolic Ca^{2+} diffusion outside this range. Secondly, we refer to the Donnan potential range, since only outside of this range is the assumption of cytosolic diffusion conditions valid. These calculations are shown in the Supplementary Material. Consequently, we define the Ca^{2+} concentration at the ith channel as $c_i = c_{\mathrm{di}}(\mathbf{r} + \Delta\mathbf{r})$. For a single open channel with flux J, Eq. 16 reduces to

$$c_i - \Omega(z_i) = \eta(\mathbf{r_i}, \mathbf{r_i} + \Delta\mathbf{r}) J = \eta_{i,i} J, \tag{19}$$

where $\eta_{i,\,i} = \eta(\mathbf{r}_i,\, \mathbf{r}_i + \Delta\mathbf{r})$. To calculate the flux J for a RyR, we insert Eq. 19 into Eq. 11b, which results in

$$\begin{aligned} J &= g(c_{\mathrm{JSR}} - c_i) = g(c_{JSR} - \Omega(z_R) - \eta_{i,i} J) \\ \Rightarrow J &= \frac{g(c_{\mathrm{JSR}} - \Omega(z_R))}{1 + g\eta_{i,i}} = g(c_{\mathrm{JSR}} - c_i) \\ \Rightarrow c_i &= \frac{g\eta_{i,i} c_{JSR} + \Omega(z_R)}{1 + g\eta_{i,i}}. \end{aligned}$$

Extending this method to a LCC immediately gives

$$\begin{aligned} J &= J_L \delta V \frac{c_{ext} \mathrm{e}^{-\delta \mathrm{V}} - \mathrm{c_i}}{1 - \mathrm{e}^{-\delta V}} \\ &= J_L \delta V \frac{c_{\mathrm{ext}} \mathrm{e}^{-\delta \mathrm{V}} - \Omega(\mathrm{z_L}) - \eta_{\mathrm{i,i}} \mathrm{J}}{1 - \mathrm{e}^{-\delta V}} \\ \Rightarrow J &= J_L \delta V \frac{(c_{\mathrm{ext}} \mathrm{e}^{-\delta \mathrm{V}} - \Omega(\mathrm{z_L}))}{J_L \delta V \eta_{i,i} + 1 - \mathrm{e}^{-\delta V}} \\ \Rightarrow c_i &= \frac{J_L \delta V \eta_{i,i} c_{\mathrm{ext}} \mathrm{e}^{-\delta \mathrm{V}} + (1 - \mathrm{e}^{-\delta \mathrm{V}}) \Omega(\mathrm{z_L})}{J_L \delta V \eta_{i,i} + 1 - \mathrm{e}^{-\delta V}}. \end{aligned}$$

The only approximation here is the use of the value of $\Delta\mathbf{r}$ calculated with a channel in the centre of the cleft (see Supplementary Material). If more than one channel is open, their Ca^{2+} concentration profiles will affect each other. This situation leads to a system of linear equations for the c_i, which is provided in the Supplementary Material.

Ca^{2+} dynamics in the JSR

We assume that the JSR has a spatially uniform Ca^{2+} concentration, which is affected by the outward flux J_{RyR} through the RyRs and the refill flux from the network sarcoplasmic reticulum (NSR). We set the timescale for refilling to $\tau_{\mathrm{refill}} = 30$ ms (Brochet et al. 2005). Moreover, we include the impact of the buffer calsequestrin on the Ca^{2+} concentration in the JSR through the fast buffer approximation, which leads to

$$\frac{\mathrm{d}c_{\mathrm{JSR}}}{\mathrm{d}t} = \beta_{\mathrm{JSR}} \left(\frac{c_{\mathrm{NSR}} - c_{\mathrm{JSR}}}{\tau_{\mathrm{refill}}} - \frac{1}{V_{\mathrm{JSR}}} \sum_j J_{\mathrm{RyR}}^{j} \right), \tag{20a}$$

$$\beta_{\mathrm{JSR}} = \left(1 + \frac{n K_c B_{\mathrm{CSQN}}}{(K_c + c_{\mathrm{JSR}})^2} \right)^{-1}, \tag{20b}$$

where n and K_C denote the number of Ca^{2+}-binding sites of calsequestrin and the dissociation constant of calsequestrin (chosen from Restrepo et al. 2008), respectively. The concentration of calsequestrin is given by B_{CSQN}.

During all simulations, we keep the Ca^{2+} concentration in the NSR, c_{NSR}, constant ($c_{\mathrm{NSR}} = 700$ μM).

Calculating the Ca^{2+} concentration at the boundary of the diadic cleft

To calculate the Ca^{2+} profile from Eq. 16, we have to determine the bulk Ca^{2+} concentration c_{bulk}. It is mainly

influenced by the diadic cleft itself. Here, we assume one point-like diadic cleft in the middle of the cell. We model the cell as a cylinder with radius $R_m = 11{,}700$ µm and length $L = 140$ µm. In addition, we take into account the pumping of Ca^{2+} from the myoplasm into the NSR via sarco-endoplasmic reticulum Ca^{2+} ATPase (SERCA) pumps, the mobile Ca^{2+} buffer calmodulin, the immobile Ca^{2+} buffer troponin and a constant leak flux J_{leak} from the NSR, which maintains a resting cytosolic Ca^{2+} concentration of 0.1 µM. This leads to

$$\frac{\partial c}{\partial t} = J\delta(r)\delta(z - L/2) + D_c\Delta c + J_{\text{leak}} - g_{\text{SERCA}}\frac{c^2}{K_m^2 + c^2} - k_+^M cM + k_-^M(B_M - M) - k_+^T cT + k_-^T(B_T - T), \tag{21a}$$

$$\frac{\partial M}{\partial t} = D_M\Delta M - k_+^M cM + k_-^M(B_M - M), \tag{21b}$$

$$\frac{\partial T}{\partial t} = -k_+^T cT + k_-^T(B_T - T), \tag{21c}$$

where B_M (B_T) and M (T) denote the total concentration of calmodulin (troponin) and the corresponding unbound concentration, respectively. The binding and unbinding of Ca^{2+} to calmodulin (troponin) is governed by $k_{\text{ac}}^{\max}$ (k_+^T) and k_-^M (k_-^T), while D_c (D_m) corresponds to the diffusion coefficient of Ca^{2+} (calmodulin). We linearize Eq. 21a, b, c around $c_{\text{rest}} = 0.1$ µM, which results in

$$\frac{\partial \delta c}{\partial t} = J\delta(r)\delta(z - L/2) + D_c\Delta\delta c - \rho_{SERCA}\delta c, -k_+^M\delta cM_0 - k_+^M\delta Mc_0 - k_+^T\delta cT_0 - k_+^T\delta Tc_0, \tag{22a}$$

$$\frac{\partial \delta M}{\partial t} = D_M\Delta\delta M - k_+^M\delta cM_0 - k_+^M\delta Mc_0, \tag{22b}$$

$$\frac{\partial \delta T}{\partial t} = -k_+^T\delta cT_0 - k_+^T\delta Tc_0. \tag{22c}$$

Here, we introduce $\delta c = c - c_{\text{rest}}$, $\delta M = M - M_0$ and $\delta T = T - T_0$, where M_0 and T_0 are the stationary buffer concentrations in the case of $c = c_{\text{rest}}$.

To solve Eq. 22a, b, c, we use the Green's function that we developed in Schendel and Falcke (2009). From simulations we notice that the bulk concentration at the boundary of the cleft can be described well by using the stationary solution. While concentrations far away from the cleft change slowly, the concentration just at the cleft rim assumes its stationary value very rapidly (Schendel and Falcke 2009). Therefore, we use once more a quasi-static approximation and arrive at a linear relation between J and c_{bulk}:

$$c_{\text{bulk}} - c_{\text{rest}} = \beta J.$$

β is a constant which follows from the solution of Eq. 22a, b, c with a three-component Green's function as presented in Schendel and Falcke (2009). This constant enters a system of linear equations (Eq. 23 in the Supplementary Material), which in turn determines c_{bulk}, c_i and J self-consistently. To summarize, we calculate the Ca^{2+} concentration at the channels and at the border of the cleft by using a quasi-static approximation and a linearization of the bulk buffering reactions outside the cleft. That reduces the problem to a system of linear equations (Eq. 23 in the Supplementary Material).

Matching the dynamics together

In the present study, we combine a deterministic description of the Ca^{2+} diffusion and the fluxes through open Ca^{2+} channels with a stochastic approach for the channel gating. Such a "mixed framework" was justified in Hake and Lines (2008) and Modchang et al. (2010). In case of comparably quick channel state transitions, the Ca^{2+} concentration in the JSR and therefore the Ca^{2+} profile in the diadic cleft remains nearly unchanged between transitions and we can use Gillespie's (1977) algorithm. If the channel transitions are slow, the Ca^{2+} concentration changes in the JSR and in the diadic cleft are not negligible and we have to use a hybrid algorithm for the stochastic simulation as described in Rüdiger et al. (2007). Our algorithm works as follows: Assume that N channel state transitions are possible with the associated propensities $\alpha_1, \ldots, \alpha_N$. Following the Gillespie algorithm, the time step τ until the next channel state transition takes place is defined by

$$\sum_i^N \alpha_i\tau = \ln 1/r_1, \tag{23}$$

where r_1 is a random number uniformly distributed in the interval [0, 1]. Note that we here assume that the propensities remain constant during the time τ. However, if the Ca^{2+} concentration in the diadic cleft changes during τ, the propensities α_i become time dependent. In this case the time τ is computed from Rüdiger et al. (2007).

$$\int_t^{t+\tau}\sum_i^N \alpha_i(s)\mathrm{d}s = \ln 1/r_1. \tag{24}$$

Results

For each simulation we applied a voltage stimulus with duration of 50 ms. For simulations with a single type of RyR cluster size we performed 80,000 simulations; for the mixed cluster size model each data point is the average of about 1,000 simulations for large clefts and about 30,000 simulations for small ones. For each simulation we acquired the time course of the Ca^{2+} currents through LCCs and RyRs. In Figs. 6 and 7 we have depicted these

Ca^{2+} currents (averaged over 80,000 simulations) for the MIN and the MAX model for diadic clefts containing 16 RyRs with membrane voltage stimulus of 0 mV.

Graded release

A valid model for a local CaRU has to reproduce general experimental results. One of the most important properties is the gradedness of Ca^{2+} release. Gradedness of Ca^{2+} release means that the amount of Ca^{2+} released from the SR changes with changing Ca^{2+} influx through the LCCs, in contrast to an all-or-non response. In Figs. 8 and 9 the maximal Ca^{2+} fluxes through LCCs and RyRs are depicted, clearly showing the existence of gradedness in both models. The maximum of the Ca^{2+} release from the SR is shifted to the left with respect to the maximum of Ca^{2+} entry through LCCs. This is due to the higher sensitivity of RyRs to higher single LCC currents [which occur following the Goldmann–Hodgkin–Katz equation (Eq. 11a) for smaller membrane potentials], reproducing experimental data (Wier et al. 1994). Both figures are obtained from simulations that account for different sizes (and accordingly different numbers of RyRs) of the diadic clefts.

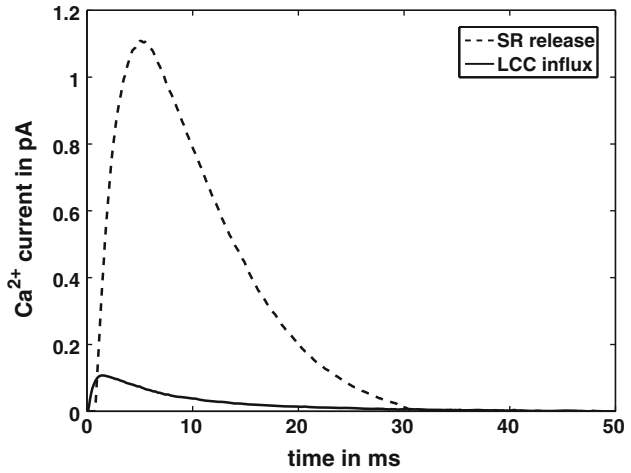

Fig. 6 Time course of Ca^{2+} currents through LCC and RyR for membrane voltage of 0 mV for the MIN model

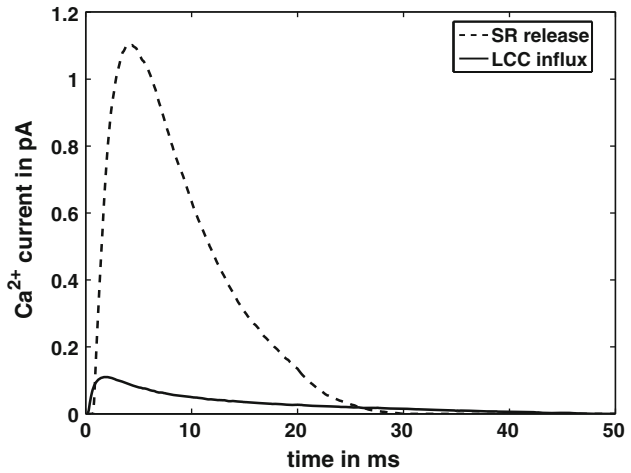

Fig. 7 Time course of Ca^{2+} currents through LCC and RyR for membrane voltage of 0 mV for the MAX model

Gain

Gain is an important physiological measure that carries information about the interaction between LCCs and RYRs. It is defined as the ratio of the maximal Ca^{2+} release flux from the SR to the maximal Ca^{2+} entry flux through LCC. In Fig. 10 we depict gain for the MIN model for two

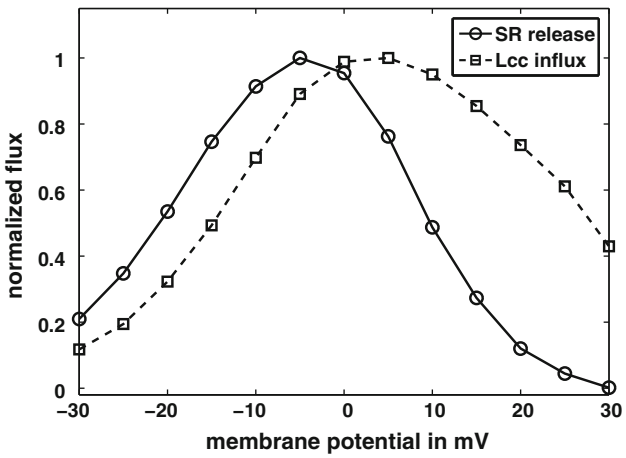

Fig. 8 Peak Ca^{2+} fluxes through RyRs and LCCs as a function of membrane potential for the MIN model. The peak for Ca^{2+} release from the SR is shifted to the left with respect to the peak of Ca^{2+} entry through LCC

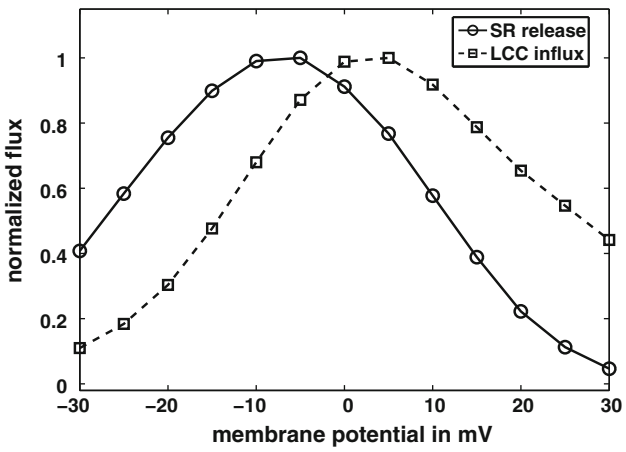

Fig. 9 Peak Ca^{2+} fluxes through RyRs and LCCs as a function of the membrane potential for the MAX model. The peak for Ca^{2+} release from the SR is shifted to the left with respect to the peak of Ca^{2+} entry through LCC

cases: We consider diadic clefts with either 16 RyRs or with exponentially distributed numbers of RyRs, with a mean of 13.6 RyRs per cleft, as outlined in the "Methods" section. The latter RyR constellation is referred to as the mixed cluster size (MCS) model in the remainder of the text. Gain has a local maximum around −25 mV in both cases. For positive membrane voltage $V > 10$ mV there is a remarkable difference between the 16-RyR diadic clefts and the MCS model, e.g. at 15 mV, gain is about 2.4 times larger in the MCS model than in the 16-RyR diad model. Also, while gain decreases quickly with increasing membrane voltage for the small cleft, the MCS model shows a slower decrease.

In Fig. 11 we depict gain for the MAX model for the 16-RyR diadic clefts and for the MCS model. Both curves increase strongly with decreasing membrane voltage. Moreover, we always have a higher gain in the MCS model than for the 16-RyR clefts. Our studies reveal that larger clefts contribute more than smaller clefts to gain. Finally, the 16-RyR clefts have again a sharp decrease of gain for positive membrane potential, while the MCS model decreases much more slowly. For example, at 15 mV, gain is about 4 times larger in the MCS model than in the 16-RyR diad model.

In Fig. 12 we compare the MCS model of the MIN and MAX models. For decreasing membrane voltage, the gain of the MAX model increases much faster than the one of the MIN model. Also, the MAX model decreases more slowly than the MIN model for positive and increasing membrane potential. Figure 13 shows a comparison between the MIN and the MAX models for the 16-RyR cleft. The increase of gain for decreasing membrane voltage is once more much higher for the MAX model, but the sharp decrease is the same for positive membrane voltage. These findings lead us to the following conclusions:

1. For high membrane potentials only diadic clefts with a large number of LCCs contribute to gain.
   An increasing membrane potential lowers the flux through the LCCs according to the Goldmann–Hodgkin–Katz equation (Eq. 11a), but increases the open probability of the LCC. Since the activation of the RyRs is a fourth-order process, the opening of one

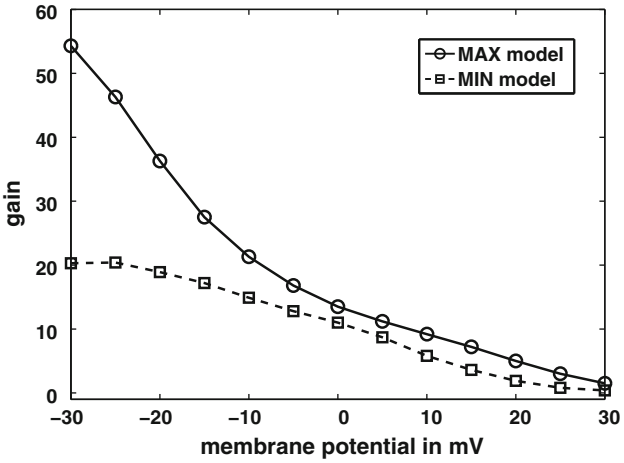

Fig. 11 Gain shown for the MAX model in case for mixed cluster size (MCS) diadic clefts (variable numbers of RyRs per cleft) (*solid line*) and in case of clefts with 16 RyRs (*dashed line*)

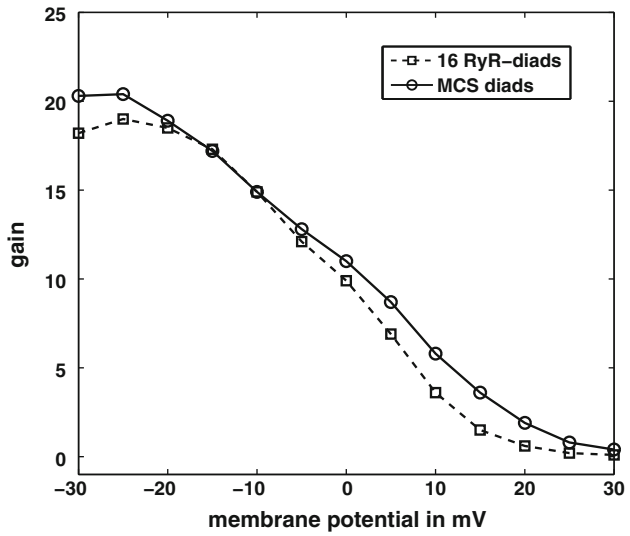

Fig. 10 Gain shown for the MIN model in case for mixed cluster size (MCS) diadic clefts (variable numbers of RyRs per cleft) (*solid line*) and in case of clefts with only 16 RyRs (*dashed line*)

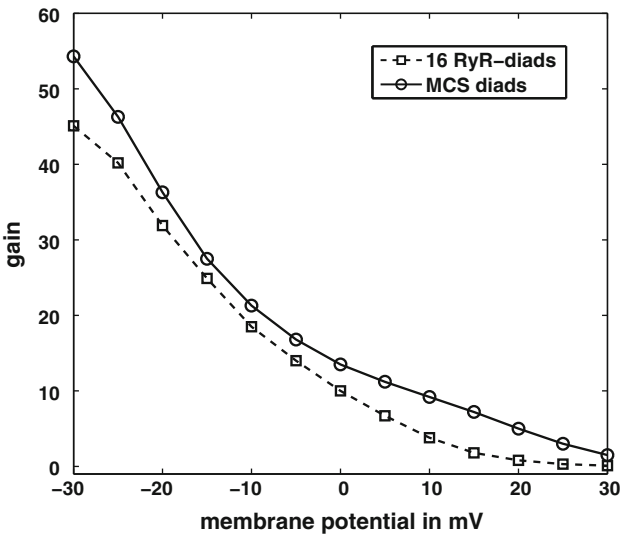

Fig. 12 Gain shown for the MAX (*solid line*) and MIN (*dashed line*) models in case of mixed cluster size (MCS) diadic clefts (variable numbers of RyRs per cleft). For decreasing membrane potential, gain increases faster in the MAX model

LCC (in the MIN model) or the opening of two LCCs (in the MAX model) cannot trigger the opening of a RyR any longer at higher membrane potentials. Simultaneous opening of more LCCs is required to activate the RyRs. Therefore, the early activation of RyRs for high membrane voltages is always a result of multiple open LCCs. Since large diadic clefts have more LCCs, the possibility of openings of several LCCs is higher than for small diadic clefts. This is also shown in Fig. 14, where diadic clefts containing 16 and 64 RyRs are compared.

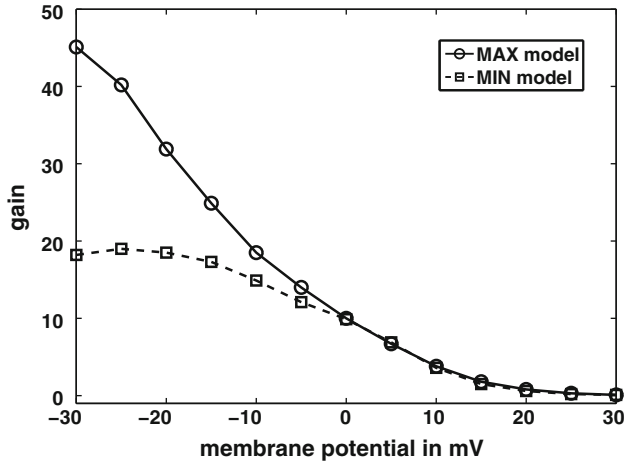

Fig. 13 Gain shown for the MAX (*solid line*) and MIN (*dashed line*) models in case for diadic clefts with 16 RyRs. For decreasing membrane potential, gain increases faster in the MAX model. For positive membrane potential, MIN and MAX model predict nearly identical values for gain

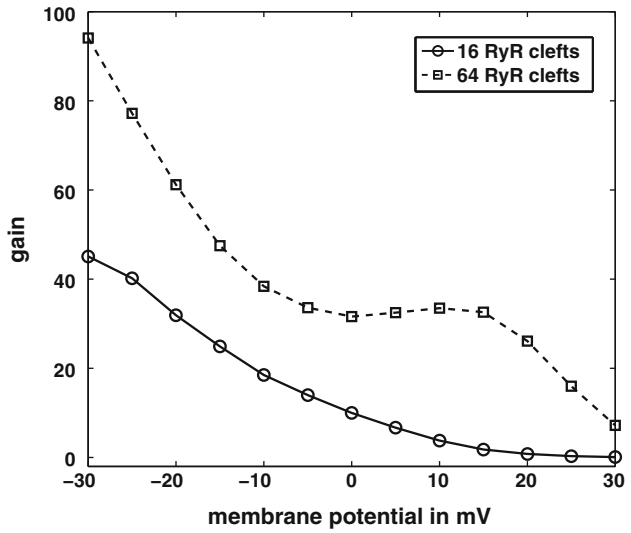

Fig. 14 Gain for diadic clefts containing 16 and 64 RyRs. The larger cleft contributes more to gain

2. The shape of the gain curve is qualitatively different depending on whether a single or multiple LCC openings (at 0 mV) are necessary to activate the RyRs. If the opening of one RyR can be efficiently triggered by the opening of one LCC (for 0 mV), the gain curve exhibits a maximum for negative membrane potentials in the voltage range where a relevant Ca^{2+} release occurs. This is a sign that the Ca^{2+} concentrations resulting from the high Ca^{2+} currents through the open LCC are large enough that the Ca^{2+} concentration at the RyRs is not a rate-limiting step for the opening of the RyRs any longer. Additionally, gain decreases rapidly for high membrane potentials. This is indicative of the fact that the simultaneous opening of multiple LCCs do not occur frequently enough to balance the reduced Ca^{2+} flux through a single LCC. If the opening of one RyR is the product of multiple LCC openings (at 0 mV), the gain curve strongly increases for decreasing negative membrane potentials. The reason is as follows: Suppose that n activated LCCs are necessary to trigger the opening of RyRs at 0 mV. Then, the activation of 1,…, $n - 1$ LCCs does not contribute substantially to the activation of RyRs, which in turn results in a lower gain. If we decrease the membrane voltage by some ΔV, the Ca^{2+} fluxes through the LCCs increase, so that $(n - 1)$ activated LCCs suffice to open the RyRs, so that CICR works more efficiently and consequently gain increases. If gain as a function of membrane voltage is a monotonically decreasing function over a wide range of the membrane potential (especially for negative values), it indicates that several LCCs have to open in order to activate RyRs. Accordingly, gain will decrease slowly for positive membrane potentials, since the decreasing Ca^{2+} flux through a single LCC can partly be compensated by the activation of $(n + 1)$, $(n + 2)$, … LCCS if (and only if) $n > 1$.

Experimental data (Wier et al. 1994 ; Song et al. 2001) show that gain strongly increases with decreasing membrane potential for negative membrane potential. Furthermore, the decrease of gain is smooth for increasing and positive membrane voltage. This suggests that, for physiological values of the membrane potential, the opening of RyRs is induced by the opening of multiple LCCs at the same time.

Influence of geometric properties and the electric field on CICR

We also study the dependence of CICR for variable distances of the JSR from the T-tubule. The gain for three

different heights is plotted in Fig. 15 for the MAX model. Gain decreases for increasing height. Since gain can be viewed (for fixed membrane potential) as an indicator of the strength of the coupling between membrane depolarisation and Ca^{2+} release, ECC decreases with increasing height of the diadic cleft. In this context the question arises how the myocyte protects itself against effects of varying geometric properties. Soeller and Cannel (1997) conclude that the electric field can be seen in many respects as a volume expansion. This corresponds to the field-dependent effective height h^* in our model, which sets currents and concentrations (Eq. 14). In Eq. 15 we found that the effective height h^* is approximately $h^* = h + 24$ nm for $h > 5$ nm and therefore larger than h. It follows that the sensitivity of h^* to changes of h, $\frac{1}{h^*}\frac{\partial h^*}{\partial h}$, is substantially smaller with an electric field than without it, as Fig. 16 shows, especially in the physiologically relevant range around 15 nm. The electric field partly compensates the effect of varying heights of the diadic cleft. In this sense, it stabilizes CICR and therefore ECC in cardiac myocytes.

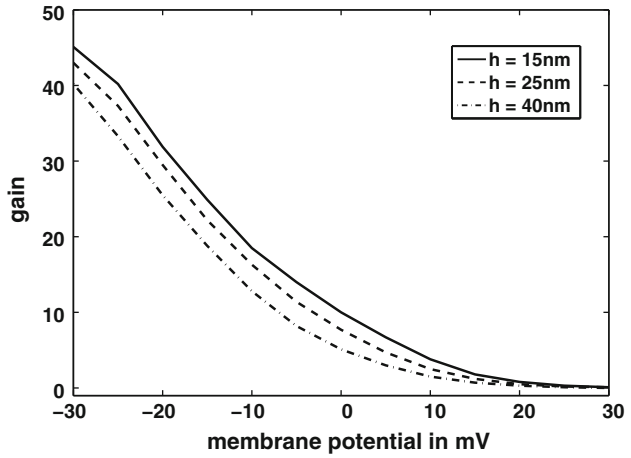

Fig. 15 Gain for different heights of the diadic cleft: $h = 15$, 25, 40 nm. The coupling decreases for increasing height

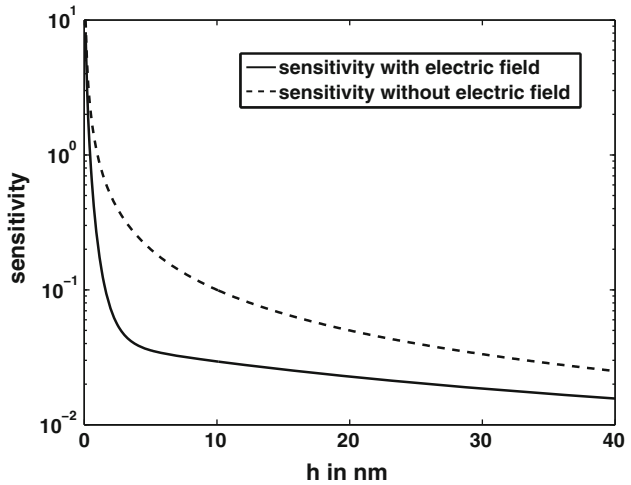

Fig. 16 The sensitivity $\frac{1}{h^*}\frac{dh^*}{dh}$ in the presence (*solid line*) and absence (*dashed line*) of an electric field as a function of the height h of the diadic cleft. The system is less sensitive to changes of h when an electric field is present

Discussion

Our study focusses on two cases of the early stage of CICR. On the one hand, we consider the possibility that one activated LCC suffices to trigger Ca^{2+} release through RyRs, while in the other case, simultaneous activation of multiple LCCs is necessary to induce the opening of RyRs. We find that both mechanisms exhibit characteristic differences in the gain curves. Comparing our results with experimental data strongly suggests that several LCCs have to be conducting to trigger activation of the RyRs. Moreover, we have shown that, for positive membrane potentials, only diadic clefts that contain many LCCs contribute substantially to gain.

The main motivation for the present study lies in contradictory experimental reports. Measurements indicate that there are on average 13.6 RyRs per RyR cluster (Baddeley et al. 2009) and that multiple open LCCs are necessary to trigger the activation of RyRs (Polakova et al. 2008). At the same time the RyR-to-LCC ratio is reported to be 4–7 (Wang et al. 2001; Bers and Stiffel 1993). As these numbers do not add up, we chose to change the number of conducting LCCs that activate RyRs to understand the impact of different RyR-to-LCC ratio rather than to extract an exact value of this ratio.

Former papers focussing on modelling CICR in the cardiac ventricular myocyte commonly assume that the opening of a RyR is triggered by the opening of a single LCC. Their gain curves match in general our findings for this mechanism. For example in Williams et al. (2007), the gain curve has a local maximum in the negative membrane voltage range and there is a sharp decrease of gain for positive membrane potential. Tanskanen et al. (2007) also report a small increase in gain for decreasing membrane potential. An exception is the paper by Greenstein and Winslow (2002), where the gain increases strongly for negative membrane voltage. We believe that this happens due to the missing saturation of the activation rate for high Ca^{2+} concentrations, which leads to the unphysiological effect of nearly immediate opening of RyRs for an open LCC.

The fact that RyR activation is a fourth-order process, i.e. four Ca^{2+} ions have to bind to the RyR for it to open, is crucial in distinguishing whether one ore more LCCs are necessary to trigger Ca^{2+} liberation from the SR. Decreasing the order of RyR activation decreases also the

number of simultaneous LCC openings required for triggering a RyR from a few to one. In respecting the physiological binding order of the RyR, the present study goes beyond earlier investigations (Hinch et al. 2004; Stern et al. 1999; Restrepo et al. 2008).

Our model is computationally inexpensive, which we achieve through a quasi-static approximation for the concentration profiles inside the diadic cleft. Due to this approximation we can replace the partial differential equation (PDE) for the Ca^{2+} concentration in the cleft by a system of linear equations whose dimension is one more than the number of Ca^{2+} releasing channels. In addition, we consider an ordinary differential equation for the Ca^{2+} concentration in the JSR. The time step of the numerical simulation is given by either the time in which the channels open and close or by the timescale of the Ca^{2+} dynamics in the JSR. This indicates that the speed up compared with the integration of a PDE is orders of magnitude, since the latter involves solving much larger systems of linear equations many times in between two channel state changes.

Like all models, our model has its specific limitations. Due to the assumption of quasi-stationary of Ca^{2+} profiles in the diadic cleft, we neglect the influence of buffers, which can delay the rise or the decrease of the Ca^{2+} concentration and hence changes the dynamics, especially on small timescales. Nevertheless, the influence of buffers in the diadic cleft is studied in Koh et al. (2006), where the authors conclude that there is no qualitative influence of the Ca^{2+} buffer on the Ca^{2+} dynamics in the diadic cleft. Moreover, Stern et al. (1999) mention that errors using the steady-state approximation can be compensated by adjusting parameters.

In the model we assumed that the low number of open RyRs is due to their rapid Ca^{2+} inactivation. However, we want to mention that in the scientific community also other possibilities are discussed. For example, the low number of open RyRs could be caused by their slow activation due to occupancy of the RyR activation sites by magnesium ions under resting conditions [for further details, see Zahradnikova et al. (2003, 2010) and Laver and Honen (2008)].

Finally, we did not include the possibility that a diadic cleft can contain more than one RyR cluster. We admit that we miss therefore the possibility that the opening of one RyR cluster can trigger the opening of other clusters within one diadic cleft. However, the scope of this article is mainly to investigate the direct coupling between LCCs and RyRs rather than the interaction between RyR clusters.

Our solution of the diffusion equation in the cleft leads to the introduction of the effective height h^*, which is larger than the geometric height and corresponds to a volume expansion. This finding expresses analytically what Soeller and Cannel (1997) report numerically in their study, where they showed that the effect of the electric field is comparable to a volume expansion. The effective height suggests a physiological role of the electric field in the diadic cleft: it partly compensates changes in the height of the diadic cleft, stabilizing CICR. We would like to speculate that this is an important and necessary mechanism of the myocyte to deal with varying cleft geometries.

We have presented here a local model of CICR, focussing on the dynamics of the CaRU, which neglects coupling between different diadic clefts. We assume that this assumption does not affect our results, which mainly focussed on gain measured on short time scales. Also, Wier et al. (1994) excluded cells exhibiting instabilities due to spatial coupling form their measurements. The definition of gain focusses on the ratio of maximal Ca^{2+} fluxes and reflects therefore the interaction between LCCs and RyRs in the diadic clefts. While of course activated RyR clusters can trigger the activation of neighbouring RyR clusters, this will not affect gain, since this effect would take too much time to influence the maximal flux values. Based on the same time scale argument, we also neglected slower feedback processes mediated by bulk $[Ca^{2+}]$, e.g. via mitochondria or slow changes of network Ca^{2+} content. We relied on Jayasinghe et al. (2009) with our assumptions that sodium–calcium exchanger (NCX) are not present in the diadic cleft. In order to build a global model of the Ca^{2+} dynamics in the myocyte, an extension by a multi-component Green's function [outlined in subsection "Calculating the Ca^{2+} concentration at the boundary of the diadic cleft" and in Schendel and Falcke (2009)] could be suitable way. Such a global model could not only account for the coupling between RyR clusters, but also include the influence of plasma membrane channels such as Ca^{2+}-ATPases and Na^+–Ca^{2+} exchangers, as well as mitochondrial Ca^{2+} uptake and the interaction between the network sarcoplasmic reticulum and the myoplasm.

Acknowledgments Thomas Schendel was supported by the International Research Training Group 1360 of the Deutsche Forschungsgemeinschaft, and Rüdiger Thul was supported by a Leverhulme Trust Early Career Fellowship.

References

Adachi-Akahane S, Cleemann L, Morad M (1999) BAY K 8644 modifies Ca^{2+} cross signaling between DHP and ryanodine receptors in rat ventricular myocytes. Am J Physiol Heart Circ Physiol 276:H1178–H1189

Altamirano J, Bers DM (2007) Voltage dependence of cardiac excitation–contraction coupling: unitary Ca^{2+} current amplitude and open channel probability. Circ Res 101:590–597

Baddeley D, Jayasinghe ID, Lam L, Rossberger S, Cannell MB, Soeller C (2009) Optical single-channel resolution imaging of the ryanodine receptor distribution in rat cardiac myocyte. Proc Natl Acad Sci USA 106:22275–22280

Bers DM, Stiffel VM (1993) Ratio of ryaodine to dihydropyridine receptors in cardiac and skeletal muscle and implications for E–C coupling. Am J Physiol Cell Physiol 264:C1587–C1593

Bers DM (2002) Cardiac excitation–contraction coupling. Nature 415:198–205

Brochet DXP, Yang DM, Maio AD, Lederer J, Franzini-Armstrong C, Cheng HP (2005) Ca^{2+} blinks: rapid nanoscopic store calcium signaling. Proc Natl Acad Sci USA 102:3099–3104

Franzini-Armstrong C, Protasi F (1997) Ryanodine receptors of striated muscles: a complex channel capable of multiple interactions. Pysiolog Rev 76:699–729

Franzini-Armstrong C, Protasi F, Ramesh V (1999) Shape, size, and disribution of Ca^{2+} release units and couplons in skeletal and cardiac muscles. Biophys J 77:1528–1539

Gillespie DT (1977) Exact stochastic simulation of coupled chemical reactions. J Phys Chem 81:2340–2361

Greenstein JL, Winslow RL (2002) An integrative model of the cardiac ventricular myocyte incorporating local control of Ca^{2+} release. Biophys J 83:2918–2945

Györke S, Györke I, Lukyanenko V, Terentyev D, Viatchenko-Karpinski S, Wiesner TF (2002) Regulation of sarcoplasmic reticulum calcium release by luminal calcium in cardiac muscle. Front Biosc 7:1454–1463

Hake J, Lines GT (2008) Stochastic binding of Ca^{2+} ions in the dyadic cleft; continuous vs. random walk description of diffusion. Biophys J 94:4184–4201

Hinch R, Greenstein JL, Tanskanen AJ, Xu L, Winslow RL (2004) A simplified local control model of calcium-induced calcium release in cardiac ventricular myocytes. Biophys J 85:3723–3736

Jayasinghe I, Cannell M, Soeller C (2009) Organization of ryanodine receptors, transverse tubules, and sodium–calcium exchanger in rat myocytes. Biophys J 97:266473

Koh X, Srinivasan B, Ching HS, Levchenko A (2006) A 3D Monte Carlo analysis of the role of dyadic space geometry in spark generation. Biophys J 90:1999–2014

Langer GA, Peskoff A (1996) Calcium concentration and movement in the diadic cleft space of the cardiac ventricular cell. Biophys J 70:1169–1182

Laver DR, Honen BN (2008) Luminal Mg^{2+}, a key factor controlling RYR2-mediated Ca^{2+} release: cytoplasmic and luminal regulation modeled in a tetrameric channel. J Gen Physiol 132:429–446

Mejia-Alvarez R, Kettlun C, Rios E, Stern M, Fill M (1999) Unitary Ca^{2+} current through cardiac ryanodine receptor channels under quasi-physiological ionic conditions. J Gen Physiol 113:177–186

Modchang C, Nadkarni S, Bartol TM, Triampo W, Sejnowski TJ, Levine H, Rappel WJ (2010) A comparison of deterministic and stochastic simulations of neuronal vesicle release models. Phys Biol 7:026008

Polakova E, Zahradnikova AJr, Pavelkova J, Zahradnik I, Zahradnikova A (2008) Local calcium release activation by DHPR calcium channel openings in rat cardiac myocytes. J Physiol 586:3839–3854

Restrepo JG, Weiss JN, Karma A (2008) Calsequestrin-mediated mechanism for cellular calcium transient alternans. Biophys J 95:3767–3789

Rüdiger S, Shuai JW, Huisinga W, Nagaiah C, Warnecke G, Parker I, Falcke M (2007) Hybrid stochastic and deterministic simulations for calcium blips. Biophys J 93:1847–1857

Schendel T, Falcke M (2009) Efficient and detailed model of the local Ca^{2+} release unit in the ventricular cardiac myocyte. Gen Inform 22:142–155

Scriven D, Dan P, Moore E (2000) Distribution of proteins implicated in excitation–contraction coupling in rat ventricular myocytes. Biophys J 79:268291

Shannon TR, Wang F, Puglisi J, Weber C, Bers DM (2004) A mathematical treatment of integrated Ca dynamics within the ventricular myocyte. Biophys J 87:3351–3371

Sobie EA, Dilly KW, Santos Cruz J, Lederer WJ, Jafri MS (2002) Termination of cardiac Ca^{2+} sparks: an investigative mathematical model of calcium-induced calcium release. Biophys J 83:59–78

Soeller C, Cannel MB (1997) Numerical simulation of local calcium movements during L-type calcium channel gating in the cardiac diad. Biophys J 73:97–111

Song LS, Wang SQ, Xiao RP, Spurgeon H, Lakkata EG, Cheng H (2001) β-Adrenergic stimulation synchronizes intracellular Ca^{2+} release during excitation–contraction coupling in cardiac myocytes. Circ Res 88:794–801

Stern MD, Song LS, Cheng H, Sham JSK, Yang HT, Boheler KR, Rios E (1999) Local control models of cardiac excitation–contraction coupling. A possible role for allosteric interactions between ryanodine receptors. J Gen Physiol 113:469–489

Tang Y, Othmer HG (1994) A model of calcium dynamics in cardiac myocytes based on the kinetics of ryanodine-sensitive calcium channels. Biophys J 67:2223–2235

Tanskanen AJ, Greenstein JL, Chen A, Sun SX, Winslow RL (2007) Protein geometry and placement in the cardiac dyad influence macroscopic properties of calcium-induced calcium release. Biophys J 92:3379–3396

Wang SQ, Song LS, Lakkata EG, Cheng H (2001) Ca^{2+} signalling between single L-type Ca^{2+} channels and ryanodine receptors in heart cells. Nature 410:592–596

Wang SQ, Stern MD, Rios E, Cheng H (2004) The quantal nature of Ca^{2+} sparks and in situ operation of the ryanodine receptor array in cardiac cells. Proc Natl Acad Sci USA 101:3979–3984

Wier WG, Egan TM, Lopez-Lopez JR, Balke CW (1994) Local control of excitation-contraction coupling in rat heart cells. J Physiol 474:463–471

Williams GSB, Huertas AH, Sobie EA, Jafri MS, and Smith GD (2007) A probabilty density approach to modeling local control of calcium-induced calcium release in cardiac myocytes. Biophys J 92:2311–2328

Zahradnikova A, Dura M, Györke I, Escobar AL, Zahradnik I, Györke S (2003) Regulation of dynamic behavior of cardiac ryanodine receptor by Mg^{2+} under simulated physiological conditions. Am J Physiol Cell Physiol 285:C1059–1070

Zahradnikova A, Valent I, Zahradnik I (2010) Frequency and release flux of calcium sparks in rat cardiac myocytes: a relation to RYR gating. J Gen Physiol 136:101–116